Extraction and verification of coherent structures in near-wall turbulence*

Hu Hai-Bao(胡海豹)†, Du Peng(杜 鹏), Huang Su-He(黄苏和), and Wang Ying(王 鹰)

School of Marine Engineering, Northwestern Polytechnical University, Xi'an 710072, *China*

(Received 29 November 2012; revised manuscript received 17 January 2013)

According to the characteristics of coherent structures in near-wall turbulence, an accurate extraction and verification method is developed based on wavelet transform (WT) and correlation analysis in this paper. At first, the fluid field of a turbulent boundary layer is measured precisely in a gravitational low-speed water tunnel. On the basis of the distribution of the coherent structures, velocity data of three test points are selected and analyzed, whose dimensionless heights are 20.8, 33.5, and 42.6. According to the frequency range of power spectrum density (PSD), coherent and incoherent structures are both extracted from the original signals using continuous and orthogonal wavelet transforms. To confirm the validity of the extracted signals, the probability density function (PDF) of each extracted signal is calculated. The result demonstrates that the incoherent structures obey the Gaussian distribution, while the coherent structures deviate from the Gaussian distribution. The PDFs of the coherent structures and the original signals are similar, which shows that the coherent structures make most contributions to the turbulence. For further verification, a correlation parameter between coherent and incoherent structures is defined, which evidently proves the validity of the extraction method in this paper.

Keywords: boundary layer, wavelet transform, power spectrum density, coherent structure

PACS: 47.27.De, 47.27.nb, 43.60.Hj **DOI:** 10.1088/1674-1056/22/7/074703

1. Introduction

Turbulence is a common but complicated phenomenon in nature. Many simulations and experiments prove that instead of a pure random process, turbulence is a process consisting of different scales of pulsation, called the coherent structure,[1–3] which is an intrinsic property of turbulence and significantly contributes to fluid entrainment and transfer of mass, momentum, and heat.[4,5] As a result, the investigation of coherent structures is of great significance for the acquaintance and control of turbulence.

The wavelet transform (WT) has been proven to be a potentially powerful tool for the detection and extraction of coherent structures.[6–9] Based on the continuous wavelet transform (CWT), Liandrant[10] and Jiang[11,12] successively put forward the maximum energy principle, which considers the reconstructed signal at the maximum energy scale as the burst events of coherent structures. Kim[13] identified the coherent structure of a flow field around a vibrating cantilever with the CWT. However, the CWT is unable to reconstruct signals if the mother wavelet function is non-orthogonal.[14–16] To overcome this problem, Longo[17] applied the discrete wavelet transform (DWT) and extracted the multiresolution turbulent structures. Compared with the CWT, the DWT is invertible and allows multiresolution analyses. Based on the DWT and a direct numerical simulation (DNS), Kadoch[18] proved that the coherent structures are able to preserve the vortical structures with only less than 4% of wavelet coefficients while retaining 99.9% of energy. However, most investigations just emphasized the disposal method of decomposed or reconstructed signals and ignored the frequency split function of the DWT. Besides, few studies tested the validity of the extracted signals.

In this study, we measure the fluid field of the turbulent boundary layer in a newly built gravitational low-speed water tunnel. To analyze the turbulent signals, we propose a procedure based on WT and correlation analysis for the extraction and verification of coherent structures. In Section 2, the experimental technique and result are presented in detail. In Section 3, the fundamental theories of turbulent structures and WT are introduced, which set the foundation of this paper. In Section 4, the extraction and verification of the coherent structure are presented. Conclusions are given in Section 5.

2. Experimental details

2.1. Experimental technique

To realize a low-speed and stable water fluid field, we specially built a gravitational low-speed water tunnel (Fig. 1). The system uses the geopotential generated by a water level difference to drive water in the experiment segment to reach a steady flow state. In the experimental system, the water speed can be adjusted continuously from 0 m/s to 2.0 m/s, the systemic error of water speed is less than 1.0%, and the turbulence intensity at the center of the experiment segment is less than 2%. As a result, this system can realize a steady fluid field in

*Project supported by the National Natural Science Foundation of China (Grant No. 51109178), the Natural Science Foundation of Shaanxi Province, China (Grant No. 2010JQ1009), and the Specialized Research Fund for the Doctoral Program of Higher Education of China (Grant No. 20116102120009).

†Corresponding author. E-mail: huhaibao@nwpu.edu.cn

© 2013 Chinese Physical Society and IOP Publishing Ltd

the experiment segment and provide favorable conditions for the hot-film probe to approach the wall.

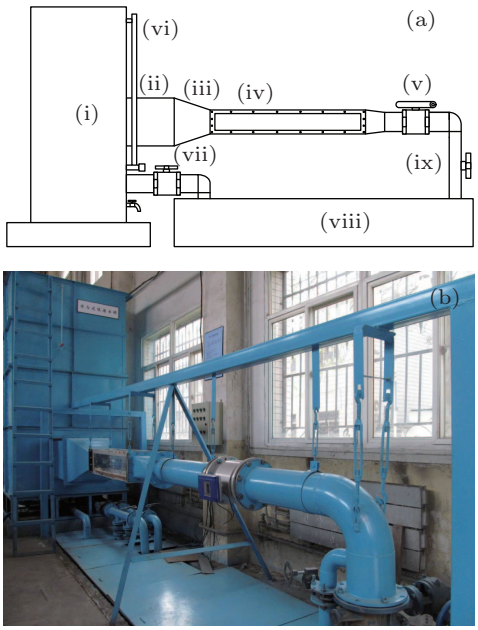


Fig. 1. (color online) (a) Sketch and (b) photo of gravitational low-speed water tunnel: (i) water tank; (ii) stabilize segment; (iii) contraction segment; (iv) experiment segment; (v) electromagnetic flowmeter; (vi) level observation segment; (vii) water pump; (viii) water storage basin; (ix) switch valve.

In the experiment, the latest IFA300 hot-wire anemometry system is used to measure the fluid field of the turbulence boundary layer. A sketch of the experimental devices is shown in Fig. 2. The coordinate frame lies right above the experiment segment. The probe stretches into water through a test hole on the top, and can be moved precisely by controlling the coordinate frame. The error is less than 0.01 mm. In the experiment, the sampling frequency is 50 kHz, and the sampling time is 10.24 s.

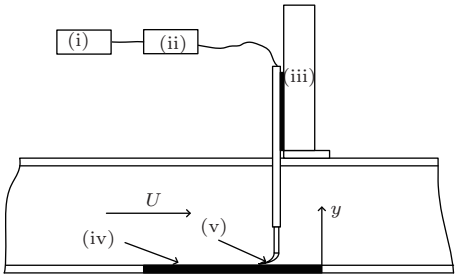


Fig. 2. Sketch of experimental devices: (i) computer; (ii) hot-wire anemometer; (iii) coordinate frame; (iv) experiment board; (v) hot-film probe.

2.2. Fluid field of a turbulent boundary layer

Based on the experimental system, we measured and studied the fluid field properties of the turbulent boundary layer. Take the profile of the mean velocity (Fig. 3) and the turbulence intensity (Fig. 4) at 0.4 m/s as example. The typical distribution of the turbulent boundary layer can be clearly observed, which proves that the fluid field in the experiment is fully developed.

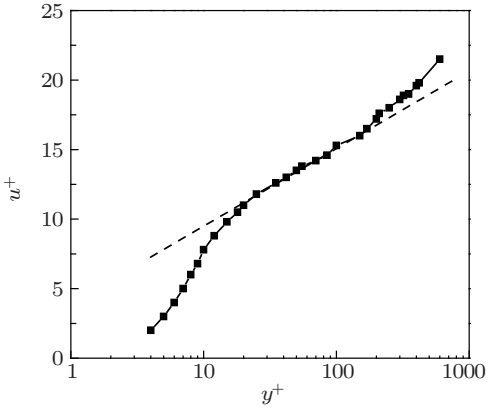


Fig. 3. Profile of mean velocity at 0.4 m/s.

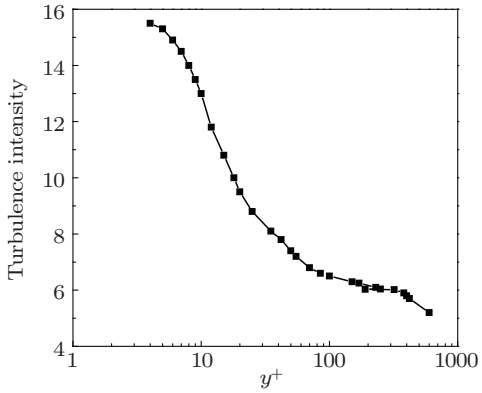


Fig. 4. Turbulence intensity at 0.4 m/s.

3. Fundamental theory

The WT of signal $s(t)$ is defined as the integral transform of $\psi_{a,b} = \frac{1}{\sqrt{a}}\psi(\frac{t-b}{a})$

$$W_{\mathrm{f}}(a,b) = \int_{-\infty}^{\infty} s(t)\psi_{a,b}\,\mathrm{d}t = \int_{-\infty}^{\infty} s(t)\frac{1}{\sqrt{a}}\psi\left(\frac{t-b}{a}\right)\mathrm{d}t, \quad (1)$$

where a is the scale parameter, and b is the position parameter.[19]

In the practical application, scale a and position b should be discretized. Usually we choose $a = 2^m$ ($m \in \mathbf{Z}$, $a_0 > 1$) and $b = n2^m$ ($b_0 > 0$, $n \in \mathbf{Z}$). When $\psi(t)$ obeys the orthogonal condition $\int \psi_{m,n}(t)\psi_{m',n'}(t)\,\mathrm{d}t = \delta_{m,m'}\delta_{n,n'}$, the set of functions forming the orthogonal basis can be written as

$$\psi_{m,n}(t) = \frac{1}{\sqrt{2^m}}\psi\left(\frac{t-n2^m}{2^m}\right) = 2^{-m/2}\psi(2^{-m}t-n). \quad (2)$$

The corresponding DWT is

$$\langle s,\psi_{m,n}\rangle = 2^{-m/2}\int_{-\infty}^{\infty} s(t)\psi_{m,n}(t)\,\mathrm{d}t = 2^{-m/2}\int_{-\infty}^{\infty} s(t)\psi(2^{-m}t-n)\,\mathrm{d}t. \quad (3)$$

The orthogonality of $\psi_{m,n}(t)$ eliminates the relevance between points in wavelet space because of the redundancy. Thus, the result of the WT can reflect the characteristics of the original signal better. Based on the orthogonal wavelet transform (OWT), signal $s(t)$ can be described as

$$s(t) = \sum_{-\infty}^{\infty}\sum_{-\infty}^{\infty}\langle s, \psi_{m,n}\rangle \psi_{m,n}(t). \tag{4}$$

Choose scale m_0 as the critical value, signal $s(t)$ can be divided into approximate and detailed parts

$$\begin{aligned} s(t) &= \sum_{m=m_0+1}^{\infty}\sum_{n=-\infty}^{\infty}\langle s, \psi_{m,n}\rangle \psi_{m,n}(t) \\ &\quad + \sum_{m=-\infty}^{m_0}\sum_{n=-\infty}^{\infty}\langle s, \psi_{m,n}\rangle \psi_{m,n}(t) \\ &= \sum_{n=-\infty}^{\infty}\langle s, \phi_{m_0,n}\rangle \phi_{m_0,n}(t) + \sum_{m=-\infty}^{m_0}\sum_{n=-\infty}^{\infty}\langle s, \psi_{m,n}\rangle \psi_{m,n}(t) \\ &= \sum_{n=-\infty}^{\infty} a_{m_0}[n]\phi_{m_0,n}(t) + \sum_{m=-\infty}^{m_0}\sum_{n=-\infty}^{\infty} d_m[n]\psi_{m,n}(t) \\ &= A_{m_0} + \sum_{m=1}^{m_0} D_m, \end{aligned} \tag{5}$$

where $\phi_{m,n}(t)$ is the scaling function, which is defined as $\phi_{m,n}(t) = 2^{-m/2}\phi(2^{-m}t - n)$, and $\psi_{m,n}(t)$ is the wavelet function. Besides, $\phi_{m,n}(t)$ works as a low-pass filter, while $\psi_{m,n}(t)$ works as a band-pass filter. The first part of Eq. (5) is the approximation (low frequency) of signal $s(t)$ at scale 2^{-m_0}, the second part is the details (high frequency) of $s(t)$.[20]

In a turbulence flow field, the fluctuating velocity signal of the turbulence can be divided into two parts

$$s = \tilde{s} + s', \tag{6}$$

where $\tilde{s}$ stands for the coherent part and s' represents the incoherent part, with $\tilde{s}$ and s' being statistically independent.

According to the WT, turbulence signal $s(t)$ can be divided into different frequency domains using the multiresolution analysis (Fig. 5). By reconstructing the signals in particular domains, which eliminate most redundant frequencies, coherent structures $\tilde{s}$ can be extracted. So the key is to calculate the frequency range of coherent structures and the frequency corresponding to each scale of the OWT, which can be obtained in the following equation:

$$f = f_c f_s / a, \tag{7}$$

where f_s is the sampling frequency, f_c is the central frequency of a particular wavelet basis, and a is the scale, whose value is 2^m (m is a particular level of decomposition) in the OWT. When m=0 (i.e., $a = 1$), $f = f_0$, which represents the original frequency range of the turbulence signal.

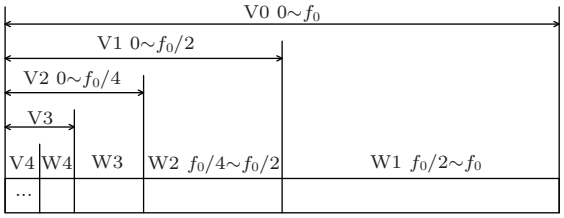


Fig. 5. Multiresolution analysis.

4. Analysis of turbulence signals

For the convenience of disposal, the signals for analysis should be selected in the centralized area of the coherent structures. The coherent structures of near-wall turbulence are essentially aroused by instability. In the development of the coherent structures, hairpin vortices are firstly formed, then hairpin vortices form strips, the instability of the strips in turn promotes the regeneration of the hairpin vortices, at last the coherent structures reach a self-sustaining cycle state. The formation of the coherent structures is in the area of $0 < y^+ < 30$, and the self-sustaining cycle mechanism is formed in the area of $20 < y^+ < 60$.[21,22] Accordingly, we analyze the velocity data of three points at 0.4 m/s, whose dimensionless heights are 20.8, 33.5, and 42.6 in the centralized area of the coherent structures. The fluctuating velocity signals of the three points are shown in Fig. 6.

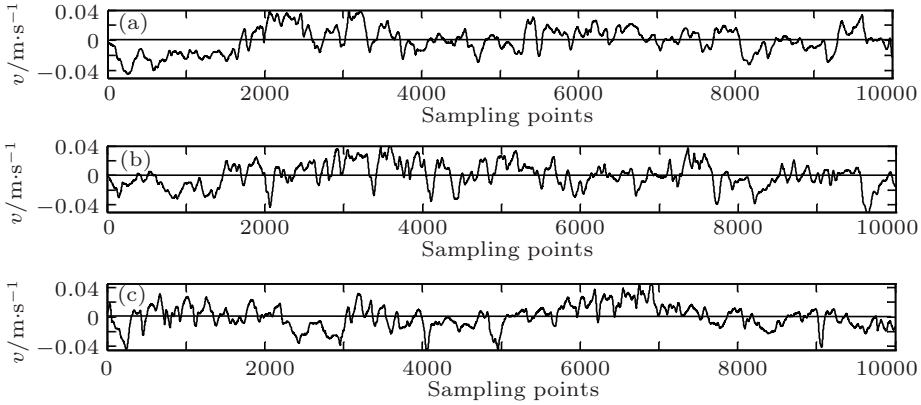


Fig. 6. Fluctuating velocity signals at (a) $y^+ = 20.8$, (b) $y^+ = 33.5$, (c) $y^+ = 42.6$.

4.1. Detection of coherent structures

To evaluate the properties of the above selected signals, we use the CWT to analyze the general situation of the coherent structures. We choose the fifth-order Daubechies wavelet as the wavelet basis, whose central frequency f_c is 0.6667 Hz. Figure 7 shows the CWT coefficients of the selected signals, which clearly show quasi-periodic structures (coherent structures) of turbulence. As a result, based on the frequency split function of the OWT, the coherent structures can be extracted once the frequency range is confirmed.

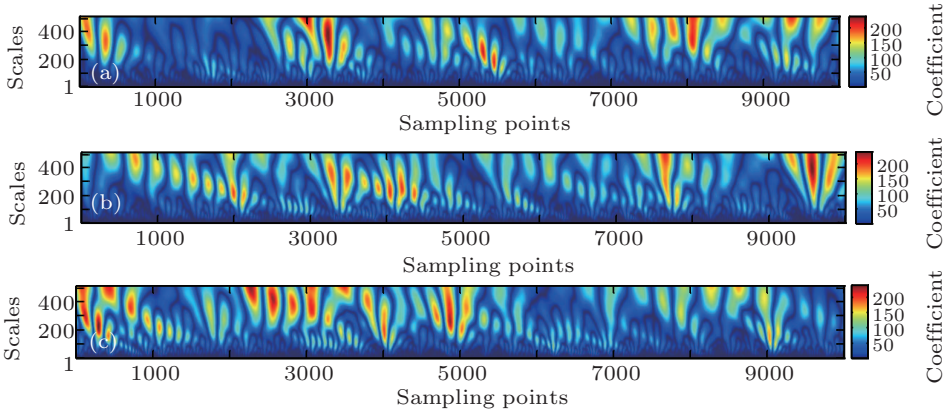


Fig. 7. (color online) CWT coefficients at (a) $y^+ = 20.8$, (b) $y^+ = 33.5$, (c) $y^+ = 42.6$.

4.2. Extraction of coherent structures

To confirm the frequency range of the coherent structures, the power spectrum density (PSD) of the selected signals is calculated (Fig. 8). It can be found that the centralized frequencies of the coherent structures are 0–230 Hz, 0–240 Hz, and 0–230 Hz, respectively. Besides, the rapid attenuation of the PSD in Fig. 8 demonstrates the low noise of the experimental system. Then, we can use the multiresolution analysis of the OWT to extract these signals as coherent structures.

Based on the OWT, the original frequency of the turbulence signal is split into 7 scales (Table 1). It can be seen that the frequency range of the approximate signal is 0–260 Hz, which covers most coherent structures. It can also be found in Table 1 that the coherent structures possess over 75% of the total energy. As a result, the best decomposition level is 7, which can eliminate most redundant signals. The extracted signals of each level are shown in Figs. 9 and 10, where A_7 in Fig. 9 is the approximate signal, i.e., coherent structures, L_7 in Fig. 10 is the incoherent structures, which is calculated by the equation

$$L_7 = s - A_7 = D_1 + D_2 + \cdots + D_7, \tag{8}$$

where s is the original signal, and D_1–D_7 are the detailed signals of each level.

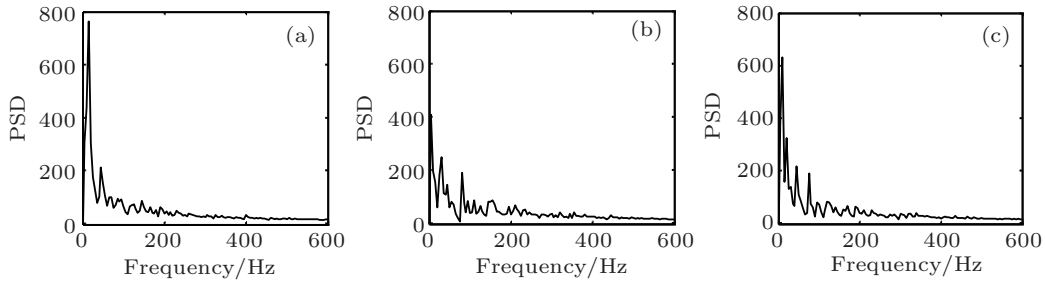


Fig. 8. Power spectrum densities at (a) $y^+ = 20.8$, (b) $y^+ = 33.5$, (c) $y^+ = 42.6$.

Table 1. Frequency and energy distribution of seven level decompositions.

	Signal	s	A_7	D_7	D_6	D_5	D_4	D_3	D_2	D_1
	Frequency/Hz	0-33335	0–260	260–520	520–1042	1042–2083	2083–4167	4167–83334	83334–16668	16668–33335
Energy/%	$y^+ = 20.8$	100	85.6498	0.0147	0.0062	0.0019	0.0464	0.3957	3.5993	10.2411
	$y^+ = 33.5$	100	77.0677	0.0200	0.0086	0.0036	0.0703	0.8099	5.5974	16.4225
	$y^+ = 42.6$	100	81.3847	0.0259	0.0129	0.0042	0.0868	0.8505	5.2322	12.4028

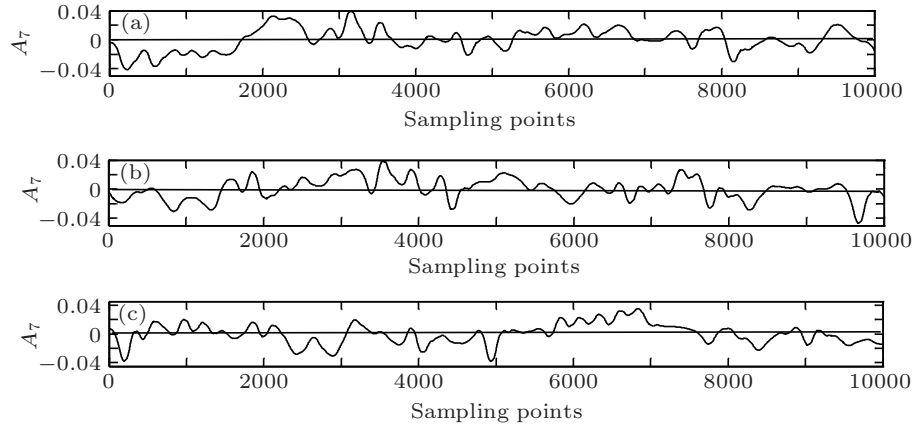


Fig. 9. Coherent structures at (a) $y^+ = 20.8$, (b) $y^+ = 33.5$, (c) $y^+ = 42.6$.

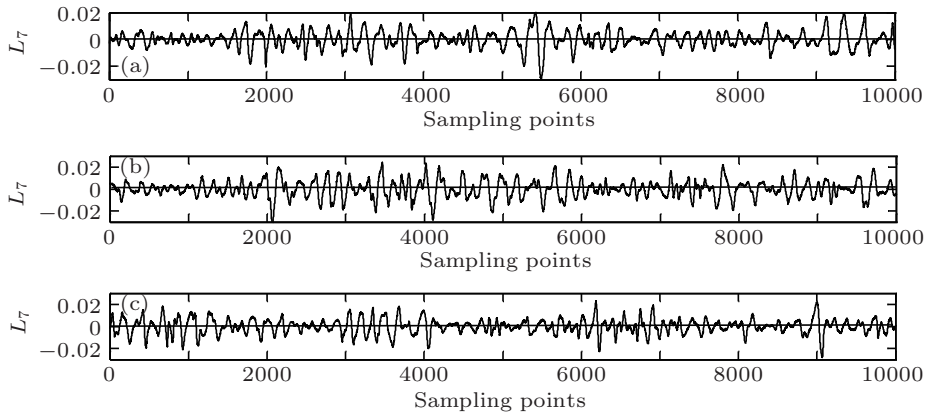


Fig. 10. Incoherent structures at (a) $y^+ = 20.8$, (b) $y^+ = 33.5$, (c) $y^+ = 42.6$.

4.3. Verification of extracted signals

To investigate the validity of the extracted signals, we firstly use the probability density function (PDF) of each signal (Fig. 11) to analyze their properties. The incoherent structures present isotropic characteristics, the signals are approximately Gaussian; while the coherent structures present strong anisotropic characteristics, and the signals are non-Gaussian and nonlinear. It can be found in Fig. 11 that the PDF of the coherent structures obviously deviates from the Gaussian distribution, and the PDF of the original signals is similar to that of the coherent structures, which demonstrates that the coherent structures make most contributions to the turbulence.

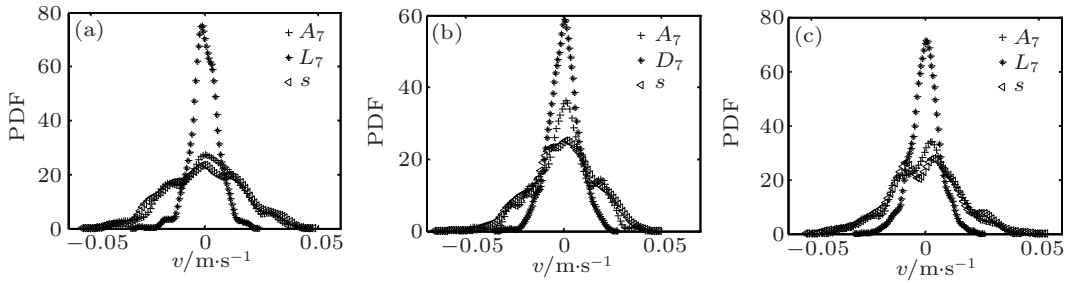


Fig. 11. Probability density functions at (a) $y^+ = 20.8$, (b) $y^+ = 33.5$, (c) $y^+ = 42.6$.

To further verify the extracted signals, according to the correlation analysis, we define a correlation parameter β between coherent and incoherent structures. Assume that the coherent structure is v_a and the incoherent structure is v_d, the equation is

$$\beta = \frac{\overline{v_\mathrm{a} v_\mathrm{d}}}{\overline{v^2}} = \frac{\sum v_{ai} v_{\mathrm{d}i}/N}{\sum v_i^2/N}, \tag{9}$$

where v is the fluctuating velocity signal, and N is the num-

ber of sampling points. The numerator $\overline{v_a v_d}$ can be approximately regarded as the stress between coherent and incoherent structures, ideally, its value should be 0. The denominator is the square of turbulence intensity. The β represents the correlation between coherent and incoherent structures. When β is large, it means that the decomposition level is so high that the coherent structures are divided into detailed signals as incoherent structures. According to Eq. (9), β of the three selected signals at level 7 are -3.8444$\times 10^{-4}$, 7.2638$\times 10^{-4}$, and 3.2677$\times 10^{-4}$, respectively, which are approximately 0. The small β demonstrates the low correlation between coherent and incoherent structures, which proves the validity of the extraction method in this paper.

5. Conclusion

In this paper, the fluid field of a turbulent boundary layer is measured in a gravitational low-speed water tunnel. To realize the accurate extraction and verification of coherent structures, a procedure based on WT and correlation analysis is put forward. The following results can be summarized.

(i) By using the frequency split function of the OWT, signals in a particular frequency range can be extracted as coherent structures.

(ii) The PDF of the incoherent structures obeys the Gaussian distribution, while the PDF of the coherent structures deviates from the Gaussian distribution. The PDFs of the original turbulence signal and the coherent structures are similar, which demonstrates that the coherent structures make most contributions to the turbulence.

(iii) A correlation parameter between coherent and incoherent structures is defined, which can be used to test the validity of the extracted signals.

References

[1] Liu J H and Jiang N 2007 *Chin. Phys. Lett.* **24** 2617
[2] Liu X B, Chen Z Q and Liu C Q 2010 *Chin. Phys. Lett.* **27** 24706
[3] Xia Z, Tian Y and Jiang N 2009 *Applied Mathematics and Mechanics* **30** 435
[4] Jiang N, Liu W, Li J H and Tian Y 2008 *Sci. China G* **38** 279
[5] Okamoto N, Yoshimatsu K, Schneider K, Farge M and Kaneda Y 2007 *Phys. Fluids* **19** 115109
[6] De Stefano G and Vasilyev O V 2012 *J. Fluid Mech.* **695** 149
[7] Futatani S, Bos W, Del-Castillo-Negrete D, Schneider K, Benkadda S and Farge M 2011 *Cr. Phys.* **12** 123
[8] Plata M D, Cant S and Prosser R 2012 *J. Comput. Phys.* **231** 6754
[9] Plata M D and Cant R S 2010 *J. Comput. Phys.* **229** 7715
[10] Liandrant J and Moret B F 1990 *Eur. J. Mech. B Fluid.* **9** 1
[11] Jiang N and Zhang J 2005 *Chin. Phys. Lett.* **22** 1968
[12] Liu J H, Jiang N, Wang Z D and Shu W 2005 *Applied Mathematics and Mechanics* **26** 495
[13] Kim Y H, Cierpka C and Wereley S T 2011 *J. Fluid Mech.* **669** 584
[14] Yoshimatsu K, Schneider K, Okamoto N, Kawahara Y and Farge M 2011 *Phys. Plasmas* **18** 092304
[15] Yao H, Sheng L F, He B and Huang J 2011 *Periodical of Ocean University of China* **41** 7
[16] Camussi R 2002 *Exp. Fluids* **32** 76
[17] Longo S 2003 *Exp. Fluids* **34** 181
[18] Kadoch B, Iyer K, Donzis D, Schneider K, Farge M and Yeung P K 2011 *J. Turbul.* **12** 1
[19] Ding G, Zhong S and Li Y 2008 *Chin. Phys. B* **17** 1998
[20] Han J J and Fu W J 2010 *Chin. Phys. B* **19** 10205
[21] Asai M, Minagawa M and Nishioka M 2002 *J. Fluid Mech.* **455** 289
[22] Chen L and Tang D B 2007 *Transactions of Nanjing University of Aeronautics & Astronautics* **24** 211